ICES Journal of Marine Science

ICES Journal of Marine Science (2019), 76(7), 2276–2285. doi:10.1093/icesjms/fsz138

Original Article

Predicting the impact of future oil-spill closures on fishery-dependent communities—a spatially explicit approach

Igal Berenshtein [1*,†], Shay O'Farrell[2*,†], Natalie Perlin[1], James N. Sanchirico[2,3], Steven A. Murawski [4], Larry Perruso[5], and Claire B. Paris[1]

[1]*Rosenstiel School of Marine and Atmospheric Science, University of Miami, 4600 Rickenbacker Causeway, Miami, FL 33149-1098, USA*
[2]*Department of Environmental Science and Policy, University of California, Davis, One Shields Avenue, Davis, CA 95616, USA*
[3]*Resources for the Future, Washington, DC 20036, USA*
[4]*University of South Florida, College of Marine Science, St. Petersburg, FL 33701, USA*
[5]*NOAA Southeast Fisheries Science Center, 75 Virginia Beach Dr, Miami, FL 33149, USA*

*Corresponding author: tel: +1 786 355 1598; e-mail: iberenshtein@rsmas.miami.edu.
†These authors have equally contributed to this work.

Berenshtein, I., O'Farrell, S., Perlin, N., Sanchirico, J. N., Murawski, S. A., Perruso, L., and Paris, C. B. Predicting the impact of future oil-spill closures on fishery-dependent communities—a spatially explicit approach. – ICES Journal of Marine Science, 76: 2276–2285.

Received 12 March 2019; revised 16 June 2019; accepted 17 June 2019; advance access publication 19 July 2019.

Major oil spills immensely impact the environment and society. Coastal fishery-dependent communities are especially at risk as their fishing grounds are susceptible to closure because of seafood contamination threat. During the *Deepwater Horizon* (*DWH*) disaster for example, vast areas of the Gulf of Mexico (GoM) were closed for fishing, resulting in coastal states losing up to a half of their fishery revenues. To predict the effect of future oil spills on fishery-dependent communities in the GoM, we develop a novel framework that combines a state-of-the-art three-dimensional oil-transport model with high-resolution spatial and temporal data for two fishing fleets—bottom longline and bandit-reel—along with data on the social vulnerability of coastal communities. We demonstrate our approach by simulating spills in the eastern and western GoM, calibrated to characteristics of the *DWH* spill. We find that the impacts of the eastern and western spills are strongest in the Florida and Texas Gulf coast counties respectively both for the bandit-reel and the bottom longline fleets. We conclude that this multi-modal spatially explicit quantitative framework is a valuable management tool for predicting the consequences of oil spills at locations throughout the Gulf, facilitating preparedness and efficient resource allocation for future oil-spill events.

Keywords: fishery management, fishery-dependent communities, oil spill, risk assessment, social vulnerability, vessel monitoring system

Introduction

The growth in global energy demands is leading to a consistent increase in offshore gas and oil exploration and extraction in deeper waters. Deeper waters are in turn more complicated for containment of a spill or an uncontrolled blowout, similar to the *Deepwater Horizon* disaster (*DWH;* Lubchenco *et al.*, 2012). During the *DWH*, ~795 million litres of oil gushed into the Gulf of Mexico (GoM) with oil slicks covering a cumulative estimated area of 149 000 km^2 (MacDonald *et al.*, 2015). As a result, vast areas of the GoM were closed to fishing, totalling an area greater than a third of the US exclusive economic zone (Ylitalo *et al.*, 2012). Consequently, commercial and recreational landings decreased by 23 and 13% respectively (Murawski *et al.*, 2016), with losses estimated at US$4.9 and US$3.5 billion (Sumaila *et al.*, 2012). In Florida's western counties, fishers resorted to travelling longer distances or relocating to ports adjacent to alternative fishing grounds. Overall, fishery landings declined by 25.3% from 2009 to 2010 (Murawski *et al.*, 2016).

Although engineering and monitoring efforts are under way to prevent another *DWH*, a fundamental challenge facing oil-spill

management is to accurately estimate the extent of a given oil spill before, during, and after it occurs, in order to evaluate trade-offs between the economic returns of the oil against the risk associated with a possible oil spill (Boehm and Page, 2007; Beyer *et al.*, 2016; Deepwater Horizon Natural Resource Damage Assessment Trustees, 2016; Nelson and Grubesic, 2018a). Most research into developing risk assessments of potential spills (Fingas, 2011; Nelson and Grubesic, 2018a) builds off of *ex post* damage assessments and outcomes of past events, e.g. area of coastline contamination, number of organisms killed, and restoration costs (Nelson *et al.*, 2015; Deepwater Horizon Natural Resource Damage Assessment Trustees, 2016; Nelson and Grubesic, 2018b). We contribute to this literature by developing an *ex ante* methodology to measure the potential impact on communities from such disasters by combining spatial dynamic modelling of a hypothetical spill with data on fishing fleet dynamics and social vulnerability of communities (Figure 1). Spatially explicit mapping of economic impacts will deepen our understanding of spills' impacts, facilitating rapid, and efficient allocation of resources to threatened communities (Jepson, 2007). Furthermore, although our focus in this paper is on the economic losses stemming from fishing, our methodology can easily be combined with other measures of economic damages (e.g. loss in tourism, biodiversity) to develop a full benefit–cost analysis that can aid in the assessment of future permitting decisions.

Methodological and technological advances allow better tracking and prediction of both oil spills and fishing fleet dynamics. The use of fishery tracking systems has rapidly increased (Deng *et al.*, 2005) and the availability of large, detailed datasets on fishing vessel movement and behaviour has provided the basis for a tool-driven revolution in fishery analytics. Artificial neural networks, random forests, hidden Markov models, and a range of other analytical tools have been successfully deployed within and across data types to understand fishing behaviour at regional and even global scales (Bastardie *et al.*, 2010; Russo *et al.*, 2011; Lambert *et al.*, 2012; Joo *et al.*, 2013; O'Farrell *et al.*, 2017; Kroodsma *et al.*, 2018), providing unprecedented insight to coastal and deep-water fishery with ever-increasing accuracy and precision.

Concurrently, advances in oil-transport simulations include implementation of key processes such as biodegradation, oil-partitioning, and evaporation into a three-dimensional Lagrangian tracking framework, which considers elements such as oceanic currents, droplet buoyancy, and wind drift (Barker, 2011; Le Hénaff *et al.*, 2012; Paris *et al.*, 2012, 2013; Boufadel *et al.*, 2014; North *et al.*, 2015; Lindo-Atichati *et al.*, 2016). Such frameworks have successfully reconstructed various aspects in the *DWH* oil spill, namely satellite footprint (Le Hénaff *et al.*, 2012; Olascoaga and Haller, 2012), shoreline contamination (Le Hénaff *et al.*, 2012; Boufadel *et al.*, 2014), evaporation (De Gouw *et al.*, 2011), sedimentation (Paris *et al.*, 2012; North *et al.*, 2015), and the formation of a deep plume (Paris *et al.*, 2012). Oil-transport models are increasingly used to estimate potential impacts of possible oil spills on the environment and economy (Nelson and Grubesic, 2018a). Most of these efforts, however, are focused on effects resulting from the direct contact of oil, considering habitats and sediment types with variable oil-retainment characteristics (Cai *et al.*, 2015; Azevedo *et al.*, 2017; Nelson and Grubesic, 2018a), and direct impacts on economic activities such as tourism (Nelson and Grubesic, 2018b). However effects such as revenue loss because of fishery closures are rarely considered in such analyses.

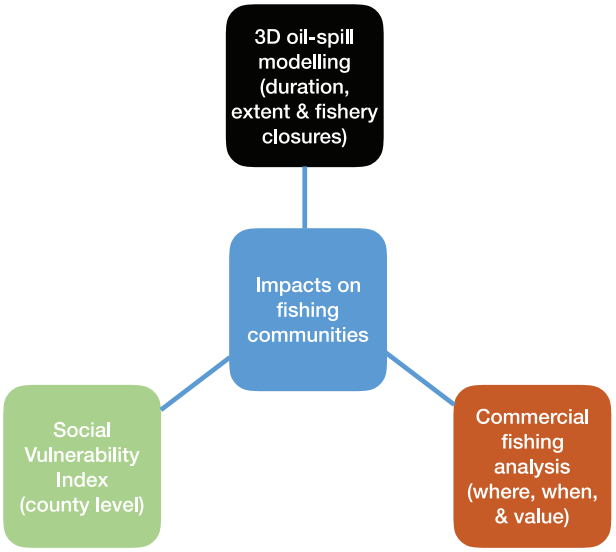

Figure 1. Multimodal spatially explicit quantitative approach composed of oil-transport, commercial fishing analysis, and social vulnerability components, and used to estimate the impact on fishing revenue losses in the aftermath of simulated oil spills and mapped to the vulnerability of the fishing communities.

Lastly, advances in social sciences introduced the social vulnerability indices (SOVIs; Cutter *et al.*, 2003)—a quantitative measure of the vulnerability of different groups given their social and economic attributes (Cutter *et al.*, 2003). These indices allow a robust evaluation of the impact of a disastrous event on a community such that more-vulnerable communities are expected to suffer a greater impact compared with more-resilient communities (Schmidtlein *et al.*, 2008). It is of policy concern not only that oil spill impacts are distributed unequally among GoM counties but also that counties may vary in their social vulnerability to environmental hazards (Cutter *et al.*, 2003). The ability to identify counties, which stand to lose larger proportions of their fishing revenue and which also have higher social vulnerability would allow the pre-emptive development of policy instruments to mitigate hardship in the event of future oil spills. We use a multimodal approach to demonstrate how the aforementioned advances can be integrated into a spatially explicit framework to predict the impact of future oil spills on fishery revenues (Figure 1). First, we deploy a three-dimensional Lagrangian oil-spill model to simulate two large spills, one each in the eastern and western GoM. We use these simulations to define closed-area boundaries based on toxic concentrations of polycyclic aromatic hydrocarbons (PAH) in the water, and allow these boundaries to change over time in response to the evolution of the plume. Second, we use data on the movement and revenue of GoM commercial reef-fish fishery vessels to estimate how compliance with the closed areas would impact fishing revenues at the county level, using a maximum loss scenario to locate the upper boundary of economic impacts. Finally, we analyse our results to identify instances where socially vulnerable counties were also heavily impacted by the loss of fishing revenue resulting from the closures.

Table 1. Simulation details, which vary between the scenarios.

Scenario	Location	Leasing block	Start date
E_GoM	27°000′N 85°168′W	The elbow	20 April 2010
W_GoM	26°660′N 93°190′W	Keathley canyon	20 April 2010

Methods

Overview

We employ a multidisciplinary approach to predict the potential impact of large oil spills on GoM fishery-dependent counties by coupling oil-transport modelling, commercial fishing analyses, and SOVIs (Figure 1).

Oil-CMS: connectivity modelling system use for oil-spill simulations

Our study implements the existing oil application (Paris *et al.*, 2012) of the connectivity modelling system (CMS; Paris *et al.*, 2013) to compute the transport and fate of the oil spilled in two hypothetical scenarios (Table 1), with blowout characteristics similar to *DWH*. *DWH*-like characteristics were applied because the duration and extent of the *DWH* spill were large enough to result in extensive fishery closures in the GoM.

The oil-CMS performs Lagrangian particle tracking of multi-fractional oil droplets released at the trap-height, i.e. the height of the first intrusion where the droplets in the buoyant jet flow lose their initial buoyancy and become neutrally buoyant (Socolofsky *et al.*, 2011). Particle transport calculations consider three-dimensional ocean currents, temperature, salinity, multi-fractional droplet buoyancy, biodegradation, dissolution, sedimentation, and surface oil evaporation. A unique fourth order Runge–Kutta spatial and temporal integration scheme forms the basis for particle advection in the oil-CMS. Computation of the terminal velocity of a droplet is based on its density, size, and Reynolds number, as well as on ambient conditions such as water temperature, salinity, density, and kinematic viscosity (Zheng *et al.*, 2003).

The model output is saved every 2 h, and includes oil droplets' effective density, size, location, and depth. The CMS horizontal grid spacing is 0.04 degrees and includes 20 vertical layers. The oil-CMS applies a multi-fractional droplet approach in which each droplet includes multiple hydrocarbon fractions (Perlin *et al.*, 2020). The biodegradation dynamics of the present study are based on high-pressure experiments and apply fraction-specific decay rates (Paris *et al.*, 2012) to account for dissolution processes where the droplet shrinks during the partitioning of oil compounds in the water column (Jaggi *et al.*, 2017). Post-processing algorithms translate model outputs into oil concentrations (Perlin *et al.*, 2020).

Experimental setup

The total amount of spilled oil in the simulations is represented in a release of 3000 oil droplets every 2 h for 90 d until 18 July 2010. The release depth is 1222 or 300 m above the Macondo well depth, the estimated trap-height (Socolofsky *et al.*, 2011). Initial droplet diameters are drawn from a uniform distribution between 1 and 500 μm. Each droplet released by the CMS model contains three pseudo-components (fractions) accounting for the differential oil density as follows: 10% light oil of 800 kg m^{-3} density, 75% intermediate oil of 840 kg m^{-3} density, and 15% heavy oil of 950 kg m^{-3} density. The biodegradation half-life rates for the light, intermediate, and heavy fractions are set to 30, 40, and 180 h, respectively, based on laboratory and observational studies (Hazen *et al.*, 2010; Schedler *et al.*, 2014; Lindo-Atichati *et al.*, 2016). Evaporation half-life rate is set to 250 h (De Gouw *et al.*, 2011) and horizontal diffusion is set to 10 m^2 s^{-1} (Okubo, 1971).

Ocean hydrodynamic forcing for the present study uses daily output from the Hybrid Coordinate Ocean Model (HYCOM; Chassignet *et al.*, 2003) for the GoM region on a 0.04 degree horizontal grid, including 40 vertical levels spanning from the surface to 5500 m. HYCOM model employs data assimilation using the Navy Coupled Ocean Data Assimilation, which assimilates available satellite altimeter and sea surface temperature observations, as well as available temperature and salinity profiles from moored buoys and ARGO floats. HYCOM output variables used for CMS simulations include horizontal and vertical velocity components, temperature, and salinity.

The simulation includes parameterization of the effects of surface wind drift (Le Hénaff *et al.*, 2012). Windstress components from the 0.5-degree Navy Operational Global Atmospheric Prediction System are interpolated into HYCOM GoM 0.04 degree grid, and 3% of their values are added to the top level ocean velocity horizontal components taking into the account the windstress rotation. The corrected ocean velocity fields are then implemented in the oil-CMS.

Oil mass and concentration estimates from the oil-CMS

To obtain oil mass and concentrations from the oil-CMS model output, information about the oil flow rate is needed. In a simplified case of the constant flow rate during the oil-spill event, a given number of total droplets released in the oil-CMS simulation, the estimated 7.3×10^5 tonne of crude oil is represented by the total of 3.132×10^6 droplets. These values translate into the 233 kg of oil represented by a single oil droplet at each release time in the oil-CMS model. Lastly, to obtain total petroleum hydrocarbons (TPH), we multiply the mass by a factor of 0.97 as TPH account for ∼97% of oil (Overton *et al.*, 2016). We approximate the droplet size distribution using the binned approach, with droplets in the same bin representing similar mass of oil per droplet, based on a lognormal distribution. We further compute the scaling factor (S_f) for each droplet as the ratio between the current and initial masses. Oil mass at each output time is then scaled to obtain effective oil mass at a given location, and summed for all the droplets found at a given time-step in each post-processing domain three-dimensional grid cell. The three-dimensional post-processing domain is of 0.02-degree resolution, with vertical layers of 0–1 m (surface layer), 2–20, 20–40,..., 2480–2500 m. After the oil mass is computed for a given droplet and a given output time, the effective oil mass from the droplets found in that grid cell at a given time are summed. Concentrations are obtained by normalizing the total oil mass to the mass of water in the corresponding grid box, producing three-dimensional concentrations across time (Perlin *et al.*, 2020).

Spill scenarios

We simulate two spill scenarios (Table 1), one in the eastern and one in the western GoM (E_GoM and W_GoM respectively) under similar conditions to the *DHW* blowout. The spill scenarios

are designed for alternative locations of a deep-sea blowout in the GoM. The locations were chosen such that the water depth is similar to that of the *DWH* accident, and thus the oil droplets are released at the same trap-height depth of 1222 m. The E_GoM site is located in the eastern part of the GoM close to the Florida peninsula and over the continental shelf break, in the "the elbow" leasing block—an area, which was recently proposed for oil exploration and production (U\.S\. Department of the Interior, 2018). The W_GoM site is located in the western part of the GoM, over an area with less steep bathymetry gradients, within the "Keathley canyon" leasing block, a petroleum-rich area in which multiple parties have leased the rights to drill (Smith, 2010).

Toxicity computation for the oil-CMS and virtual fishery closures

Toxicity computations for the oil-CMS are based on the recent finding of the toxicity amplification because of the combined effect of PAH and ultraviolet radiation, phototoxicity (Lay *et al.*, 2015), with PAH becoming toxic to early life stages of marine organisms from a concentration of $PAH = 0.5$ ppb at the surface and $PAH = 1$ ppb in deeper waters (Deepwater Horizon Natural Resource Damage Assessment Trustees, 2016). Another recently discovered toxic pathway is cardiotoxicity, i.e. the adverse effect of PAH on heart development and function in fish embryos and larvae (Deepwater Horizon Natural Resource Damage Assessment Trustees, 2016). For cardiotoxicity, the toxicity threshold is $PAH = 1$ ppb as well (Deepwater Horizon Natural Resource Damage Assessment Trustees, 2016). We apply a linear regression to compute the PAH–TPH linear relationship from the Gulf Science Data (GSD), producing the following regression equations:

$$\log_{10}(\mathrm{TPH}+1) = 1.733 + 1.0074 \times \log_{10}(\mathrm{PAH}+1) \text{ for surface.} \quad (1)$$

$$\log_{10}(\mathrm{TPH}+1) = 1.58357 + 0.85257 \times \log_{10}(\mathrm{PAH}+1) \text{ for the water column.} \quad (2)$$

More information about the toxicity computation is in the Supplementary Section S1.

Daily closures are applied as a boundary of all grid cells that contain toxic concentrations in the GoM (Figure 2) as computed by the oil-CMS model. The cumulative closures for both scenarios are determined as the boundary of all daily closures per scenario. MATLAB R2017b is used for all spatial analyses.

Fisheries data analysis

Three fisheries datasets are used in the analysis, which is conducted in *R* version 3.4.3 (R Foundation, 2017). First, we use a positional and behavioural dataset that is gathered by the on-board fishery observer programme. These *observer data* are recorded on a subset of trips by the GoM reef-fish fleet, where independent on-board observers record the time and location when fishing gears are deployed and recovered. Second, a vessel monitoring system (*VMS*) dataset provides positional information with approximately hourly resolution. *VMS* equipment has been mandated on all GoM commercial fishing vessels with a reef fish licence since 2006, irrespective of vessel size. Finally, revenue, gear type and county-of-landing data are collated from mandatory *logbook* records. Integration of the three datasets (Figure 3) is outlined below.

Data processing

Vessels that are actively engaged in fishing display characteristic movement patterns as they deploy and recover gears (Bastardie *et al.*, 2010). These movement patterns can be decomposed into quantifiable components of a vessel track, such as velocities and turning angles. The movement variables can then be combined with additional exogenous variables such as depth at location and time of day to create signature sets of variables from which fishing activity can be identified in vessel tracks (O'Farrell *et al.*, 2017). First, *VMS* data are processed to calculate the relevant movement metrics. The distances and turning angles of successive *VMS* legs are calculated using the spherical trigonometry functions and in the *R*-package, *geosphere* (Hijmans, 2016). These distances and the *VMS* time intervals are then used to calculate velocity. Time of day is extracted directly from the *VMS* signal. After processing, the derived variables are used to classify the *VMS* records into either fishing or non-fishing, using a random forest classifier that had been trained to recognize fishing behaviour using the ground-truthed fishery observer dataset. Full details of *VMS* data processing and the random forest training and testing protocol are described in O'Farrell *et al.* (2017).

Calculating lost revenue by vessel and by county

To estimate an upper bound on the economic impacts from the spill, a maximum loss scenario is used whereby any fishing that took place within the simulated closed areas is assumed to be "lost." This is a maximum loss, because we would expect that these displaced vessels would have moved to areas outside the closed areas to fish and thereby would mitigate some of the losses. For each day of the simulated oil spill, the relevant toxic concentration polygon(s) are intersected with the *VMS* fishing records for that day using the *R*-packages *sp* (Bivand *et al.*, 2013) and *raster* (Hijmans, 2017). Fishing locations that fell within the polygons are identified, and lost fishing is quantified for each trip as the proportion of *VMS* records that fell within the polygons relative to the total number of fishing records for that trip. The reported revenue in the merged logbook dataset is then adjusted accordingly. For instance, if 30% of the *VMS* fishing records for a vessel on a given trip falls within the polygon(s), it is assumed that 30% of the reported revenue is lost. Finally, losses are aggregated at county level using the merged logbook dataset, which records the county where each trip is landed. County shapefiles are downloaded from the United States Census Bureau website (2018) and imported to *R* using the package *rgdal* (Bivand *et al.*, 2017).

Fishing analyses

After merging the logbook and *VMS* datasets, 101 bottom longline trips and 222 bandit-reel trips are available (Table 2). There is a considerable spatial overlap of fishing grounds between the two fleets, which is to be expected considering that both target reef fish, albeit of differing species. Bandit-reel vessels originate in more than twice as many counties ($N = 26$) as bottom longline vessels ($N = 11$; Table 1) and the number of bandit-reel vessels

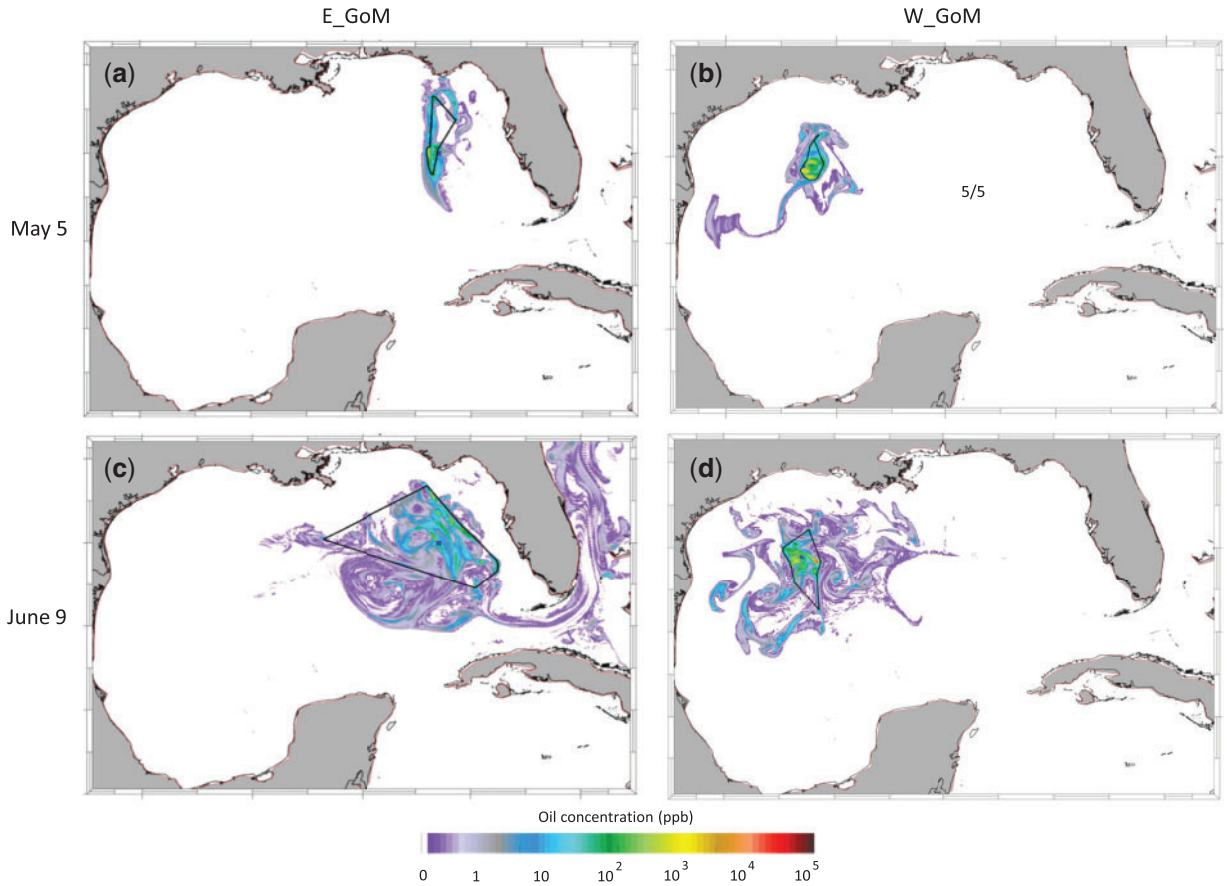

Figure 2. Daily snapshots of a simulated oil spill for the eastern (E_GoM) and western (W_GoM) spill scenarios during (a, b) 5 May 2010; (c, d) 29 June 2010. Polygons represent simulated fishery closures encompassing polycyclic aromatic hydrocarbons (PAH) concentrations higher than 0.5 ppb at the surface (depth: 0–1 m) and 1 ppb at deeper waters.

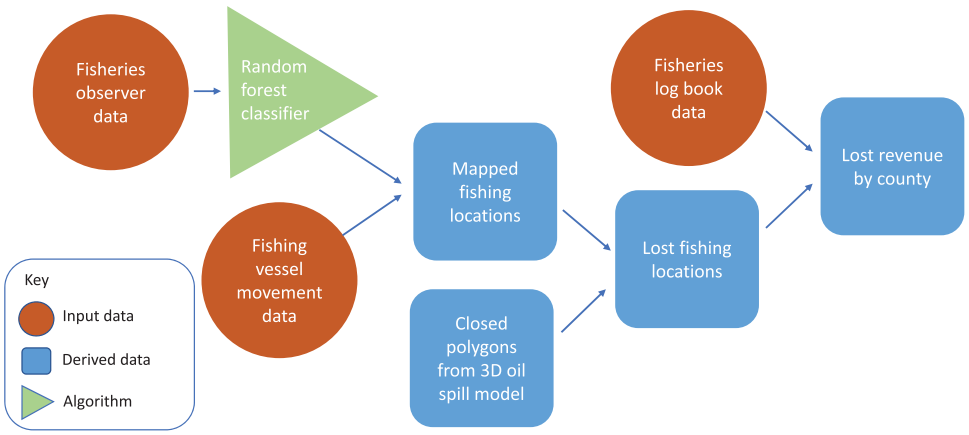

Figure 3. Fisheries data analysis process.

($N = 359$) is an order of magnitude greater than the number of bottom longline vessels ($N = 38$; Table 2).

Linking oil-spill economic impacts to social vulnerability

The *SOVI* (Cutter *et al.*, 2003) provides a numerical social vulnerability score for each US County based on 29 variables derived primarily from the US Census Bureau. The variables include metrics of wealth, social status, gender, age, ethnicity, and health insurance, among others. The dimensionality of the dataset is reduced to eight significant components using principal components analysis, and the cardinalities of the components are then adjusted so that higher *SOVI* scores indicate greater vulnerability. We focus only on the counties that border the GoM.

To identify impacted counties in revenue losses and social vulnerability, we cross-reference the *SOVI* (2010–2014) scores for

Table 2. Summary statistics of merged logbook and *VMS* datasets for two Gulf of Mexico reef-fish fleets during the simulated oil-spill fishery closures.

Fleet	Number of vessels	Number of VMS records—fishing only	Number of VMS records—total[a]	Number of fishing trips	Number of counties
Bottom longline	38	31 179	123 685	101	11
Bandit-reel	359	70 301	481 391	222	26

[a]Includes VMS records classified as "in port" and "at sea but not fishing" (e.g. steaming).

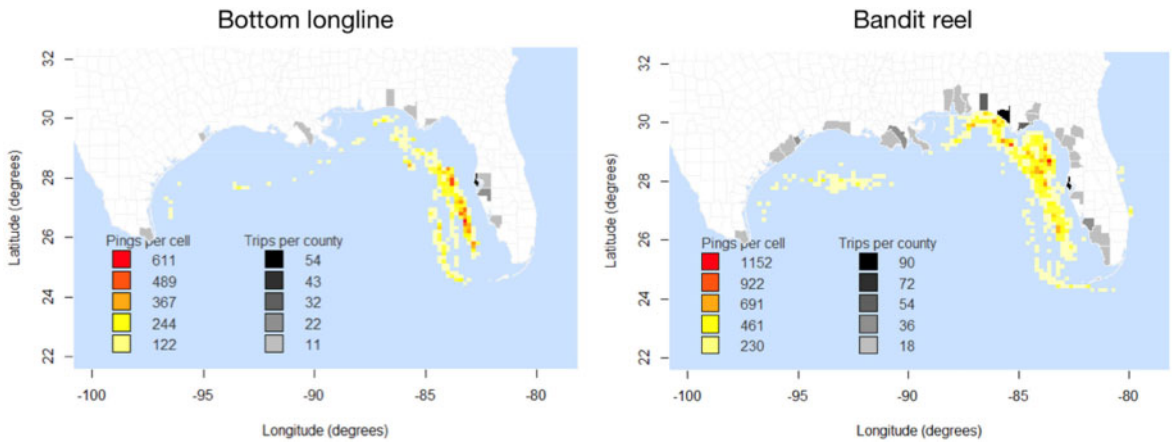

Figure 4. Fishing activity in the Gulf of Mexico (GoM) during the simulated oil spills. Coloured heatmaps show the density of fishing activity for bottom longline and bandit-reel. Greyscale heatmaps indicate the total number of trips made per county per fishery during the simulated spill period, including trips that did not overlap with the simulated closures and would therefore not have been impacted. To maintain confidentiality, fishing grid cells containing data from fewer than three vessels are not plotted. GoM states include Florida (FL), Alabama (AL), Mississippi (MS), Louisiana (LA), and Texas (TX).

each county in our study with the predicted revenue losses resulting from the two spill scenarios for the two gear types. Revenues and *SOVI* variables (V) were standardized for each impacted county, i, relative to all fishing counties, k, for each combination of a given spill (S) and fishing gear type (G_1, G_2):

$$V_{i,G_1|S} = \frac{V_{i,G_1} - \mu_{k,G_1,G_2}}{\sigma_{k,G_1,G_2}}, \tag{3}$$

where μ_{k,G_1,G_2} is the mean revenue or *SOVI* across all fishing counties, k, and gear types, and σ_{k,G_1,G_2} is the standard deviation. The *SOVI* score is originally calculated as a relative measure of social vulnerability for a large number of counties, most of which were not engaged in bandit or longline fishing during our study period. Consequently, we standardize the *SOVI* score to express the values relative only to counties in our study. A standardized *SOVI* score of zero is the average score for the counties in our study, and scores above or below zero respectively indicate counties that are above or below average vulnerability in our study. Using this standardization, we can partition the counties into four categories based on whether they lie above/below the means for both *SOVI* and revenue. For example, a county could have higher fishing revenues and at the same time be one of the most socially vulnerable counties bordering the GoM.

Results

Commercial fishing data analysis indicates that bottom longline fishing in the GoM is dominated by the Florida counties, and is concentrated on the West Florida Shelf. In contrast, bandit-reel fishing is more widespread across counties from all GoM states (Figure 4), and the fishing activity in the Gulf is also more widespread compared with bottom longline.

The Florida shelf spill (E_GoM) had a particularly large impact on socially vulnerable counties, which engage in longline fishing, with five impacted bottom longline counties (Figure 5, white triangles) being either within or bordering the red quadrant of highest concern. At the other end of the spectrum, the Texas spill (W_GoM) had a low impact on longlining counties, with only a single impacted county of below average social vulnerability (black triangle). For bandit-reel fishing the effect was milder, with two socially vulnerable counties impacted in the E_GoM (white circles), and one in the W_GoM (black circles).

Cumulative oil spill extents of the two scenarios reveal a large spread covering more than half of the GoM waters (Figure 6). Toxic concentrations of the E_GoM and W_GoM were limited, covering the eastern and the northwestern areas of the GoM respectively. In E_GoM, a considerable amount of oil entered the Gulf Stream, transporting the oil northwards along the east Florida shelf, whereas for W_GoM, oil did not enter the Gulf Stream. The relative impact because of the fishery closures is evident across counties from most GoM states, mainly Florida for E_GoM, and Texas for W_GoM (Figure 6). Relatively vulnerable counties, which suffered high revenue loss are in south Texas and central- and north-Florida (Figure 6, red shading). The effect on the bandit-reel fishery is wider across counties compared with the Bottom longline fishery, however most impacted counties are characterized by either low revenue loss and low vulnerability

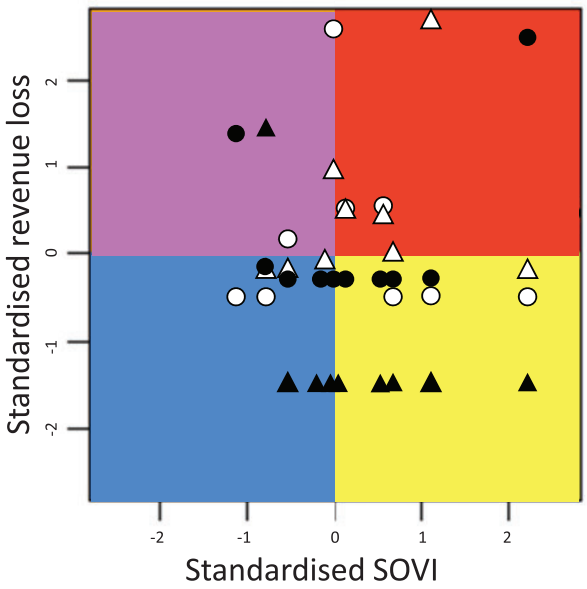

Figure 5. Fishing revenue losses vs. social vulnerability index (*SOVI*) scores for counties impacted by the two oil-spill scenarios. Values are expressed in standard deviations, with zero representing the average for all fishing counties, impacted or not. Higher SOVI scores indicate greater social vulnerability to environmental hazards. Marker shapes show gear types (triangles, bottom longline; circles, bandit-reel) and shading indicates spill scenario (white, E_GoM; black, W_GoM). Counties falling within the blue (lower left) quadrant are those that suffered relatively little revenue losses and are of low social vulnerability, and therefore may be considered of the lowest concern. Counties in the red (upper right) quadrant are those that suffered relatively high revenue losses and are also of high social vulnerability, and are thus of the highest concern. Yellow and magenta quadrants represent high *SOVI* + low revenue losses and low *SOVI* + high revenue losses, respectively.

(blue) or low revenue loss and high vulnerability (yellow). Counties with high revenue loss and low vulnerability (magenta) are in located in northern Texas and northern Florida.

Discussion

Our study demonstrates that coupling a three-dimensional oil-spill model with fishery vessel movement data, and SOVIs permit estimation of county level impacts for given oil-spill scenarios. The E_GoM and W_GoM are realistic and relevant oil scenarios as they are situated both in active and under-consideration leasing blocks. We show that Florida counties will be affected by the E_GoM and Texas counties will be mainly affected by the W_GoM scenario, yet fishing counties from other GoM states are at some risk of impact as the choice of fishing grounds is dynamic. This study provides a glimpse into how each county is susceptible to each spill scenario (Figure 6), providing important insights at the county management level, facilitating a better understanding of the risk associated with the possible spill scenarios. Similarly, these data are valuable for the fishers themselves, allowing them to anticipate and prepare their own firm-level contingency plans for a possible major spill.

The implementation of high-resolution vessel tracking systems such as *VMSs* and automatic identification system heralds a new era in fishery management (Russo *et al.*, 2011). Prior to these systems, the spatial management of fishery was mostly limited to self-reported data, which were assigned to coarse-scale management zones ("statistical areas"), constraining their usefulness. Modern tracking systems not only permit fishing vessel locations to be pinpointed with GPS-level accuracy, but also permit vessel activity to be inferred from movement and environmental variables (Bastardie *et al.*, 2010). Deploying analytical tools such as machine-learning algorithms and hidden Markov models have delivered greatly increased accuracy over traditional approaches such as speed filters (Joo *et al.*, 2013; O'Farrell *et al.*, 2017) and even allows métiers to be inferred directly from vessel data (Russo *et al.*, 2011). Although further improvements in the data and analytical methods are necessary—and indeed under way—the quality of the outputs is now sufficient that integration with spatial tools such as three-dimensional oil-spill models as well as with datasets such as habitat maps can create flexible analytical frameworks that hold great promise for fishery science and policy.

The 2010–2014 *SOVI* score we use in our manuscript is calculated from 29 variables, including per capita income and percentage of the population employed in extractive industries such as fishing. Although we plot *SOVI* scores against fishing revenues for impacted counties, we do not model either variable as a function of the other because measures of revenue would be included in both the predictors and the response. Regardless of endogeneity concerns, however, any correlation between the *SOVI* score and fishery revenue is likely to be small given that *SOVI* is calculated using numerous non-revenue variables (e.g. age, ethnicity, gender). We formally confirm that no significant correlation exists by calculating Pearson correlation coefficients for the *SOVI* scores and bandit revenues ($rho = -0.02$; $p = 0.917$) and for *SOVI* scores and longline revenues ($rho = 0.4$; $p = 0.223$).

The *SOVI* score collapses complex, high-dimensional socio-economic information into a tractable scalar quantity. Naturally, there are drawbacks in doing so. Some workers have found the scores are sensitive to the selection of variables and their representation, as well as to the relative weighting of the variables used in calculating the index (Jones and Andrey, 2007). The adaptability of the methodology to contexts beyond the United States is also questionable (Boruff and Cutter, 2007). However, in conducting a formal sensitivity analysis on *SOVI* within its geographic context, Schmidtlein *et al.* (2008) found the index to be mostly robust. *SOVI* has also been lauded for its approach to integrating theory, conceptualization, and variable selection (Adger *et al.*, 2005; Füssel, 2007). When applied in the geographical context in which the index was developed, the index lends itself well to mapping vulnerability across space (Cutter and Finch, 2008), as we have done in our study.

We chose to use the bandit-reel and longline reef-fish fishery for a number of reasons. First, both fishery had the *VMS* system installed for a number of years prior to our study period, ameliorating concerns about data quality problems during system implementation and mitigating any short-term behavioural changes induced by the recent installation of any monitoring system. Second, bandit-reel and longline are two of the dominant gear types in the GoM, comprising relatively large fleets and increasing the number of vessels that would have been fishing during our simulated study period. And third, the bandit-reel and longline reef-fish fishery employ a large number of individuals in the coastal counties of the GoM, and are thus part of a tightly coupled social-ecological system that may be considered particularly vulnerable to disturbances such as oil spills.

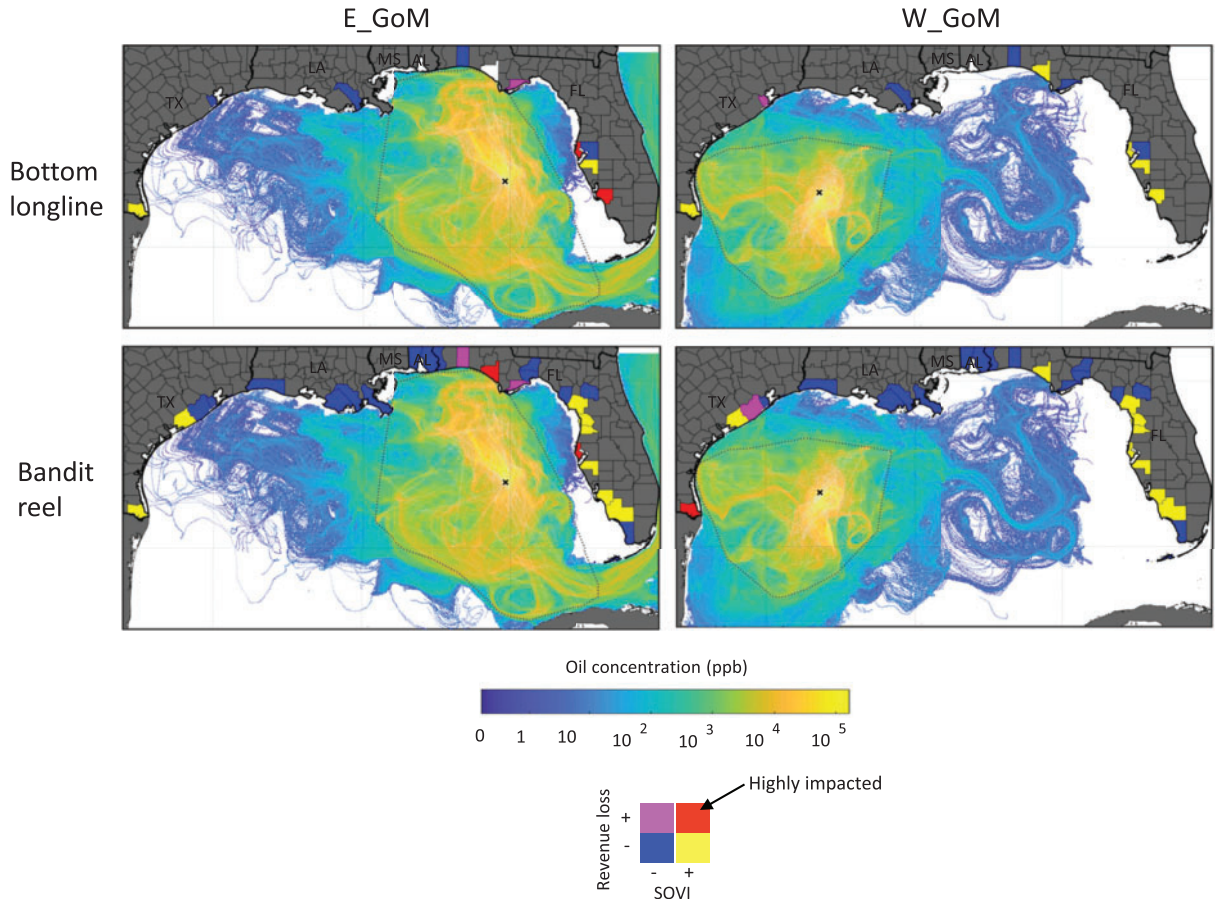

Figure 6. Relative impact of the simulated oil spills on the Gulf of Mexico (GoM) counties given fishing revenue loss and social vulnerability indices (*SOVIs*) during the simulated spill period. "+" and "−" represent above and below the mean value, with colours similar to Figure 5. E_GoM and W_GoM are simulated oil spills on the east and west GoM of the same magnitude as the *Deepwater Horizon* spill. The location of the simulated wellhead is marked with "x." Black dotted polygons are the boundary of all daily closures per scenario. Fishing gear categories include bandit-reel and bottom longline. GoM states include Florida (FL), Alabama (AL), Mississippi (MS), Louisiana (LA), and Texas (TX).

The spills simulated here represent relevant scenarios in areas, which include active leases (Smith, 2010; U\.S\. Department of the Interior, 2018; Li and Johnson, 2019). These locations provide a good spatial geographical coverage for the US region of the GoM (Figure 6). The similarity to the *DWH* in spill characteristics provides a vivid point of reference as for the possible outcomes of such spills, as well as representing ultra-deep blowout scenarios, which are difficult to contain and are therefore susceptible for longer spill durations. Future work will explore hypothetical spills with variable characteristics including other locations, different depths, spill durations, and flow-rates.

Our framework is also relevant of marine spatial planning (MSP; Douvere, 2008), an integrated management approach, which emerged in response to increasing pressure on marine natural resources (Millennium Ecosystem Assessment, 2005). MSP aims to balance stakeholder activities, which spatially interact with each other and with the marine environment, e.g. fishery, offshore petroleum industry, and shipping. This is especially relevant in environments such as the GoM, in which highly productive fishery and oil extraction infrastructure often overlap, resulting in immense anthropogenic pressure, with millions of people exploiting its resources for livelihood, energy, and nutrition (Yáñez-Arancibia and Day, 2004). By predicting the spatial distribution of water-borne pollutants and the socio-economic consequences for fishery-dependent coastal populations, our framework can provide valuable inputs to a regional GoM MSP process within frameworks such as the Gulf of Mexico Alliance, which promotes the use of ecosystem-based management at a regional level, considering ecological, social, and economic short- and long-term objectives (Carollo and Reed, 2010). Our framework would allow stakeholders to estimate the socio-economic impacts of an oil spill at a given location, varying parameters such as the magnitude or duration of the spill. The various outputs can be used as impact "visualizations" during scenario planning, helping stakeholders to make informed decisions considering the consequences of allowing oil wells to be positioned at various locations.

Our study synthesizes physical, behavioural, and socio-economic data from multiple sources to understand how oil spills could affect fishing-dependent communities in the GoM. We quantify and evaluate our results in a spatial context, providing a useful framework not only for federal policy-makers, but also for state, county, and firm-level management. Examining the spatially explicit impacts revealed by this framework can facilitate efficient allocation of resources to impacted counties in case of a major oil spill and in planning for further oil extraction in the

GoM. Future work includes incorporation of finer elements within counties and communities, including a more granular spatial analysis of the level of dependence on fishery (Jacob *et al.*, 2010), as well as integrating spatially explicit discrete-choice models to improve predictions of fishing displacement by oil spills (Berman, 2006).

Supplementary data

Supplementary material is available at the *ICESJMS* online version of the manuscript.

Acknowledgements

We thank Elizabeth Scott-Denton at the SEFSC Galveston Lab for providing the observer data on which the random forest classifier was trained and tested. The study was funded by: (i) the National Academies of Sciences—Gulf Research Programme (NAS—GRP) award: Understanding oil spill impacts on fishing communities of the Gulf of Mexico: from Deepwater Horizon to future spill scenarios (SAM, CPB, and JNS). (ii) NSF Coastal SEES grant number (1325452 to SAM and JNS). The scientific results and conclusions, as well as any views or opinions expressed herein, are those of the authors and do not necessarily reflect the views of NOAA or the United States Department of Commerce.

References

Adger, W. N., Brooks, N., Bentham, G., Agnew, M., and Eriksen, S. 2005. New indicators of vulnerability and adaptive capacity. Technical Report 7, Tyndall Centre for Climate Change Research, University of East Anglia, Norwich, Norfolk, UK.

Azevedo, A., Fortunato, A. B., Epifânio, B., den Boer, S., Oliveira, E. R., Alves, F. L., de Jesus, G. *et al.* 2017. An oil risk management system based on high-resolution hazard and vulnerability calculations. Ocean & Coastal Management, 136: 1–18.

Barker, C. H. 2011. A statistical outlook for the Deepwater Horizon oil spill. Monitoring and Modeling the Deepwater Horizon Oil Spill: A Record-Breaking Enterprise, 195: 237–244.

Bastardie, F., Nielsen, J. R., Ulrich, C., Egekvist, J., and Degel, H. 2010. Detailed mapping of fishing effort and landings by coupling fishing logbooks with satellite-recorded vessel geo-location. Fisheries Research, 106: 41–53.

Berman, M. 2006. Modeling spatial choice in ocean fisheries. Marine Resource Economics, 21: 375–394.

Beyer, J., Trannum, H. C., Bakke, T., Hodson, P. V., and Collier, T. K. 2016. Environmental effects of the Deepwater Horizon oil spill: a review. Marine Pollution Bulletin, 110: 28–51.

Bivand, R., Keitt, T., and Rowlingson, B. 2017. rgdal: Bindings for the Geospatial Data Abstraction Library. R package.

Bivand, R. S., Pebesma, E., and Gómez-Rubio, V. 2013. Applied Spatial Data Analysis with R. Springer New York, New York.

Boehm, P. D., and Page, D. S. 2007. Exposure elements in oil spill risk and natural resource damage assessments: a review. Human and Ecological Risk Assessment: An International Journal, 13: 418–448.

Boruff, B. J., and Cutter, S. L. 2007. The environmental vulnerability of Caribbean island nations. Geographical Review, 97: 24–45.

Boufadel, M. C., Abdollahi-Nasab, A., Geng, X., Galt, J., and Torlapati, J. 2014. Simulation of the landfall of the Deepwater Horizon oil on the shorelines of the Gulf of Mexico. Environmental Science & Technology, 48: 9496–9505.

Cai, L., Yan, L., Ni, J., Wang, C., Cai, L., Yan, L., Ni, J. *et al.* 2015. Assessment of ecological vulnerability under oil spill stress. Sustainability, 7: 13073–13084.

Carollo, C., and Reed, D. J. 2010. Ecosystem-based management institutional design: balance between federal, state, and local governments within the Gulf of Mexico Alliance. Marine Policy, 34: 178–181.

Chassignet, E. P., Smith, L. T., Halliwell, G. R., and Bleck, R. 2003. North Atlantic simulations with the hybrid coordinate ocean model (HYCOM): impact of the vertical coordinate choice, reference pressure, and thermobaricity. Journal of Physical Oceanography, 33: 2504–2526.

Cutter, S. L., Boruff, B. J., and Shirley, W. L. 2003. Social vulnerability to environmental hazards. Social Science Quarterly, 84: 242–261.

Cutter, S. L., and Finch, C. 2008. Temporal and spatial changes in social vulnerability to natural hazards. Proceedings of the National Academy of Sciences of the United States of America, 105: 2301–2306.

De Gouw, J. A., Middlebrook, A. M., Warneke, C., Ahmadov, R., Atlas, E. L., Bahreini, R., Blake, D. R. *et al.* 2011. Organic aerosol formation downwind from the Deepwater Horizon oil spill. Science, 331: 1295–1299.

Deepwater Horizon Natural Resource Damage Assessment Trustees. 2016. Deepwater Horizon Oil Spill: Final Programmatic Damage Assessment and Restoration Plan and Final Programmatic Environmental Impact Statement.

Deng, R., Dichmont, C., Milton, D., Haywood, M., Vance, D., Hall, N., and Die, D. 2005. Can vessel monitoring system data also be used to study trawling intensity and population depletion? The example of Australia's northern prawn fishery. Canadian Journal of Fisheries and Aquatic Sciences, 62: 611–622.

Douvere, F. 2008. The importance of marine spatial planning in advancing ecosystem-based sea use management. Marine Policy, 32: 762–771.

Fingas, M. F. 2011. Oil Spill Science and Technology: Prevention, Response, and Clean up. Gulf Professional Publisher/Elsevier, Burlington, MA. 1156 pp.

Füssel, H-M. 2007. Vulnerability: a generally applicable conceptual framework for climate change research. Global Environmental Change, 17: 155–167.

Hazen, T. C., Dubinsky, E. A., DeSantis, T. Z., Andersen, G. L., Piceno, Y. M., Singh, N., Jansson, J. K. *et al.* 2010. Deep-sea oil plume enriches indigenous oil-degrading bacteria. Science (New York, N.Y.), 330: 204–208.

Hijmans, R. J. 2016. Geosphere: Spherical Trigonometry. R package.

Hijmans, R. J. 2017. Raster: Geographic Data Analysis and Modeling. R package.

Jacob, S., Weeks, P., Blount, B. G., and Jepson, M. 2010. Exploring fishing dependence in gulf coast communities. Marine Policy, 34: 1307–1314.

Jaggi, A., Snowdon, R. W., Stopford, A., Radović, J. R., Oldenburg, T. B. P., and Larter, S. R. 2017. Experimental simulation of crude oil-water partitioning behavior of BTEX compounds during a deep submarine oil spill. Organic Geochemistry, 108: 1–8.

Jepson, M. 2007. Social indicators and measurements of vulnerability for Gulf Coast fishing communities. NAPA Bulletin, 28: 57–68.

Jones, B., and Andrey, J. 2007. Vulnerability index construction: methodological choices and their influence on identifying vulnerable neighbourhoods. International Journal of Emergency Management, 4: 269–295.

Joo, R., Bertrand, S., Tam, J., and Fablet, R. 2013. Hidden Markov Models: the best models for forager movements? PLoS One, 8: e71246.

Kroodsma, D. A., Mayorga, J., Hochberg, T., Miller, N. A., Boerder, K., Ferretti, F., Wilson, A. *et al.* 2018. Tracking the global footprint of fisheries. Science (New York, N.Y.), 359: 904–908.

Lambert, G. I., Jennings, S., Hiddink, J. G., Hintzen, N. T., Hinz, H., Kaiser, M. J., and Murray, L. G. 2012. Implications of using alternative methods of vessel monitoring system (VMS) data analysis to describe fishing activities and impacts. ICES Journal of Marine Science, 69: 682–693.

Lay, C. R., Morris, J. M., Takeshita, R., Forth, H. P., Travers, C. L., Roberts, A. P., Alloy, M. *et al.* 2015. The Effect of Ultraviolet (UV) Radiation on the Toxicity of Deepwater Horizon Oil (TOX_TR.12). DWH Toxicity NRDA Technical Working Group Report, Boulder, CO.

Le Hénaff, M., Kourafalou, V. H., Paris, C. B., Helgers, J., Aman, Z. M., Hogan, P. J., and Srinivasan, A. 2012. Surface evolution of the Deepwater Horizon oil spill patch: combined effects of circulation and wind-induced drift. Environmental Science & Technology, 46: 7267–7273.

Li, Z., and Johnson, W. 2019. An improved method to estimate the probability of oil spill contact to environmental resources in the Gulf of Mexico. Journal of Marine Science and Engineering, 7: 41.

Lindo-Atichati, D., Paris, C. B., Le Hénaff, M., Schedler, M., Valladares Juárez, A. G., and Müller, R. 2016. Simulating the effects of droplet size, high-pressure biodegradation, and variable flow rate on the subsea evolution of deep plumes from the Macondo blowout. Deep-Sea Research Part II: Topical Studies in Oceanography, 129: 301–310.

Lubchenco, J., McNutt, M. K., Dreyfus, G., Murawski, S. A., Kennedy, D. M., Anastas, P. T., Chu, S. *et al.* 2012. Science in support of the Deepwater Horizon response. Proceedings of the National Academy of Sciences of the United States of America, 109: 20212–20221.

MacDonald, I. R., Garcia-Pineda, O., Beet, A., Daneshgar Asl, S., Feng, L., Graettinger, G., French-McCay, D. *et al.* 2015. Natural and unnatural oil slicks in the Gulf of Mexico. Journal of Geophysical Research: Oceans, 120: 8364–8380.

Millennium Ecosystem Assessment. 2005. Living beyond Our Means: Natural Assets and Human Well-Being. Statement from the Board. UNEP, Paris, France.

Murawski, S., Fleeger, J., Patterson, III, W. , Hu, C., Daly, K., Romero, I., and Toro-Farmer, G. 2016. How did the oil spill affect coastal and continental Deepwater Horizon shelf ecosystems of the Gulf of Mexico? Oceanography, 29: 160–173.

Nelson, J. R., and Grubesic, T. H. 2018a. Oil spill modeling. Progress in Physical Geography: Earth and Environment, 42: 112–127.

Nelson, J. R., and Grubesic, T. H. 2018b. The implications of oil exploration off the Gulf Coast of Florida. Journal of Marine Science and Engineering, 6: 30.

Nelson, J. R., Grubesic, T. H., Sim, L., Rose, K., and Graham, J. 2015. Approach for assessing coastal vulnerability to oil spills for prevention and readiness using GIS and the blowout and spill occurrence model. Ocean & Coastal Management, 112: 1–11.

North, E. W., Adams, E. E., Thessen, A. E., Schlag, Z., He, R., Socolofsky, S. A., Masutani, S. M. *et al.* 2015. The influence of droplet size and biodegradation on the transport of subsurface oil droplets during the Deepwater Horizon spill: a model sensitivity study. Environmental Research Letters, 10: 024016.

O'Farrell, S., Sanchirico, J. N., Chollett, I., Cockrell, M., Murawski, S. A., Watson, J. T., Haynie, A. *et al.* 2017. Improving detection of short-duration fishing behaviour in vessel tracks by feature engineering of training data. ICES Journal of Marine Science, 74: 1428–1436.

Okubo, A. 1971. Oceanic diffusion diagrams. Deep Sea Research and Oceanographic Abstracts, 18: 789–802.

Olascoaga, M. J., and Haller, G. 2012. Forecasting sudden changes in environmental pollution patterns. Proceedings of the National Academy of Sciences of the United States of America, 109: 4738–4743.

Overton, E., Wade, T., Radovic, J., Meyer, B., Miles, M. S., and Larter, S. 2016. Chemical composition of Macondo and other crude oils and compositional alterations during oil spills. Oceanography, 29: 50–63.

Paris, C. B., Helgers, J., Van Sebille, E., and Srinivasan, A. 2013. Connectivity modeling system: a probabilistic modeling tool for the multi-scale tracking of biotic and abiotic variability in the ocean. Environmental Modelling & Software, 42: 47–54.

Paris, C. B., Hénaff, M., Le, Aman, Z. M., Subramaniam, A., Helgers, J., Wang, D. P., Kourafalou, V. H. *et al.* 2012. Evolution of the Macondo well blowout: simulating the effects of the circulation and synthetic dispersants on the subsea oil transport. Environmental Science and Technology, 46: 13293–13302.

Perlin, N., Paris, C. B., Berenshtein, I., Vaz, A. C., Faillettaz, R., Aman, Z. M., Schwing, P. *et al.* 2020. Far-field modeling of deep-sea blowout: sensitivity studies of initial conditions, biodegradation, sedimentation and SSDI on surface slicks and oil plume concentrations. *In* Deep Oil Spills. Ed. by S. Murawski, C. Ainsworth, S. Gilbert, D. Hollander, C. Paris, M. Schlüter and D. Wetzel. Springer, pp. 170–192.

R Foundation. 2017. The R Project for Statistical Computing. Vienna. https://www.r-project.org/ (last accessed 9 April 2018).

Russo, T., Parisi, A., Prorgi, M., Boccoli, F., Cignini, I., Tordoni, M., and Cataudella, S. 2011. When behaviour reveals activity: assigning fishing effort to métiers based on VMS data using artificial neural networks. Fisheries Research, 111: 53–64.

Schedler, M., Hiessl, R., Valladares Juárez, A. G., Gust, G., and Müller, R. 2014. Effect of high pressure on hydrocarbon-degrading bacteria. AMB Express, 4: 77.

Schmidtlein, M. C., Deutsch, R. C., Piegorsch, W. W., and Cutter, S. L. 2008. A sensitivity analysis of the social vulnerability index. Risk Analysis: An International Journal, 28: 1099–1114.

Smith, T. 2010. GOM: more giant oil discoveries. GeoExPro: 62. https://www.geoexpro.com/magazine/vol-7-no-2 (last accessed 18 September 2018).

Socolofsky, S. A., Adams, E. E., and Sherwood, C. R. 2011. Formation dynamics of subsurface hydrocarbon intrusions following the Deepwater Horizon blowout. Geophysical Research Letters, 38: n/a.

Sumaila, U. R., Cisneros-Montemayor, A. M., Dyck, A., Huang, L., Cheung, W., Jacquet, J., Kleisner, K. *et al.* 2012. Impact of the *Deepwater Horizon* well blowout on the economics of US Gulf fisheries. Canadian Journal of Fisheries and Aquatic Sciences, 69: 499–510.

U.S. Department of the Interior. 2018. Secretary Zinke Announces Plan For Unleashing America's Offshore Oil and Gas Potential | U.S. Department of the Interior. https://www.doi.gov/pressreleases/secretary-zinke-announces-plan-unleashing-americas-offshore-oil-and-gas-potential (last accessed 18 September 2018).

Yáñez-Arancibia, A., and Day, J. W. 2004. The Gulf of Mexico: towards an integration of coastal management with large marine ecosystem management. Ocean & Coastal Management, 47: 537–563.

Ylitalo, G. M., Krahn, M. M., Dickhoff, W. W., Stein, J. E., Walker, C. C., Lassitter, C. L., Garrett, E. S. *et al.* 2012. Federal seafood safety response to the Deepwater Horizon oil spill. Proceedings of the National Academy of Sciences of the United States of America, 109: 20274–20279.

Zheng, L., Yapa, P. D., and Chen, F. 2003. A model for simulating deepwater oil and gas blowouts—part I: theory and model formulation. Journal of Hydraulic Research, 41: 339–351.

Handling editor: Mark Gibbs